JMATPRO	Journal of Advanced Materials and Processing 9 (4): 13-22, Autumn 2021 http://jmatpro.iaun.ac.ir 20.1001.1.2322388.2021.9.4.2.4

Research Paper

Polymer-Assisted Synthesis and Characterization of Nickel Aluminate Nanoparticles for Photodegradation of Methylene Blue

Sogol Bakhtiarvand, Seyed Ali Hassanzadeh-Tabrizi*,
Advanced Materials Research Center, Department of Materials Engineering, Najafabad Branch, Islamic Azad University, Najafabad, Iran

ARTICLE INFO

Article history:

Received 26 August 2021
Accepted 2 October 2021
Available online 1 November 2021

Keywords:
NiAl2O4
Nanopowders
Photocatalytic activity
Wet chemical method

ABSTRACT

A simple polymer-assisted wet chemical method was used to synthesize $NiAl_2O_4$ nanopowder. The photocatalytic properties of synthesized powders were investigated for the degradation of methylene blue. For this aim, metal salts and polymeric precursors were dissolved in water, and then a crosslinker was added till a gel was formed. The product was calcined to produce nanopowders. XRD results confirmed the formation of nickel aluminate with spinel structure. In addition, the findings showed that the produced $NiAl_2O_4$ nanopowders have a particle size range between 35 to 100 nm with a uniform particle size distribution. The optical properties of the samples showed that the bandgap energy of $NiAl_2O_4$ is about 3.44 eV. The nickel aluminate nanopowders demonstrated high photocatalytic activity for photodegradation of methylene blue, which could be attributed to their small particle sizes. It seems that the polymer-assisted wet chemical synthesis may open up an effective route for the production of ceramic photocatalyst nanopowders with high quality.

Citation: Bakhtiarvand, S., Hassanzadeh-Tabrizi, S.A., (2021) Polymer-Assisted Synthesis and Characterization of Nickel Aluminate Nanoparticles for Photodegradation of Methylene Blue, Journal of Advanced Materials and Processing, 9 (4), 13-22. Dor: 20.1001.1.2322388.2021.9.4.2.4

* Corresponding Author.
E-mail address: hassanzadeh@pmt.iaun.ac.ir

1. Introduction

The water contamination by organic dies produced by different industries like textile is an important problem in Today's communities. It was reported these contaminants could cause lots of problems for human beings and alive ecosystems. For example, different kinds of gastric diseases and cancers are some issues caused by these organic dyes in the drinking water [1–3]. In addition, the lives of many aquatic animals would be endangered. Many methods have been used to remove these dangerous materials from water. One of the promising methods is the photodegradation of organic dyes on the surface of ceramic semiconductors. These semiconductors harvest the energy of the light and create reactive specious, which attack the structure of molecules and degrade them to the less dangerous compounds like water and carbon dioxide molecules. Due to the high potential of photocatalyst technology, new and complex semiconductors are in great demand [4–6].

Nanostructured ceramic oxides have gotten a lot of attention because of their potential utilization in different industries as semiconductors, pigments, electrical devices, and catalytic nanomaterials. Nickel aluminate ($NiAl_2O_4$) belongs to the spinel groups of ceramics, with the general formula AB_2O_4, where A and B are divalent and trivalent cations, respectively [7,8]. $NiAl_2O_4$ is widely used in catalytic applications ranging from methanol-reforming to hydrocarbon cracking, dehydrogenation, photodegradation, etc. [7,9–11]. In addition, $NiAl_2O_4$ is used as a pigment in the industry [12]. By doping nickel aluminate with different metallic cations, it is possible to manipulate the optical properties of this spinel and create different colors. The solid-state process, the sol-gel technique, and wet chemical approaches such as hydrothermal and solvothermal procedures may all be used to make $NiAl_2O_4$. The polymer-assisted synthesis method is a method based on combining polymeric monomers and a crosslinker. A polymeric gel is formed due to a free radical polymerization reaction which traps materials inside its structure. This method has the ability to produce nanomaterials with controlled sizes and structures [13–16].

Although nickel aluminate nanoparticles were synthesized via different methods, there is no report on the synthesis of this material via the polymeric gel route. Therefore, a simple polymer-assisted wet chemical method was utilized to produce $NiAl_2O_4$ nanopowders. Afterward, the photocatalytic activity of produced powders was studied for the photodegradation of methylene blue.

2. Experimental procedure

2.1. Materials and method

The $NiAl_2O_4$ nanopowders were made using a polymer-assisted gel process, which involved dissolving $Ni(NO_3)\cdot 6H_2O$ (1.36 g) and $Al(NO_3)_3\cdot 9H_2O$ (4.2 g) in 20 ml distilled water. Ni/Al had a molar ratio of 1/2. N,N'-methylene-bis-acrylamide (MBAM), Acrylamide (AM), and ammonium persulfate (AP) were utilized as raw materials for the formation of the gel. The AM (9.18 g) and MBAM (0.41 g) were added to the metal ions solution. After the AM and MBAM were dissolved, AP (0.35 g) was added to the solution. The mole ratio of AM/MBAM/AP was 24/2/1. The prepared solution was stirred until a gel was obtained. Then the gel was dried at 80 °C and calcined at 800 °C for 2 h in the air at a heating rate of 5 °C/min.

2.2. Characterization

An X-ray diffraction analysis (Philips PW3040) with Cu-Kα radiation was used to investigate the structure of the $NiAl_2O_4$ nanopowder. A DTA-TGA analyzer was used to evaluate the samples' thermal behavior (SDT Q600, STA Instruments). An X-ray diffractometer was used to examine the sample's crystalline structure progression (Philips PW3040). Fourier Transformed Infrared spectra (FTIR) in the range of 400–4000 cm^{-1} were recorded using a JASCO FTIR 4100 instrument. The optical characteristics were investigated using UV–Visible diffuse reflectance spectroscopy (JASCO-V670 spectrophotometer). The size and form of the nanoparticles were observed using SEM (VEGA/TESCAN Mira 3-XMU) and TEM (Philips-Model: MC 30).

2.3. Photocatalytic activity of the samples

Methylene blue was used as a contaminant organic dye model to evaluate the photocatalytic properties of synthesized samples. A 25 mL glass beaker was filled with 10 mL of 2 mg/L methylene blue solution (pH=7) containing 0.4 g/L of the nickel aluminate powder. UV lamps positioned at 10 cm of the cell were used to irradiate the suspension. To achieve a homogenous mixture of samples, the suspension was continually agitated. The absorption at 664 nm was used to estimate the amount of methylene blue in the solution using a UV−vis spectrophotometer. The photodegradation percent was calculated using equation 1.

$$Photodegradation\ percent = (C_1\text{-}C_2)/C_1 * 100 \quad \text{(Eq. 1)}$$

where C_1 and C_2 are the initial amounts of methylene blue at times t_0 and t, respectively.

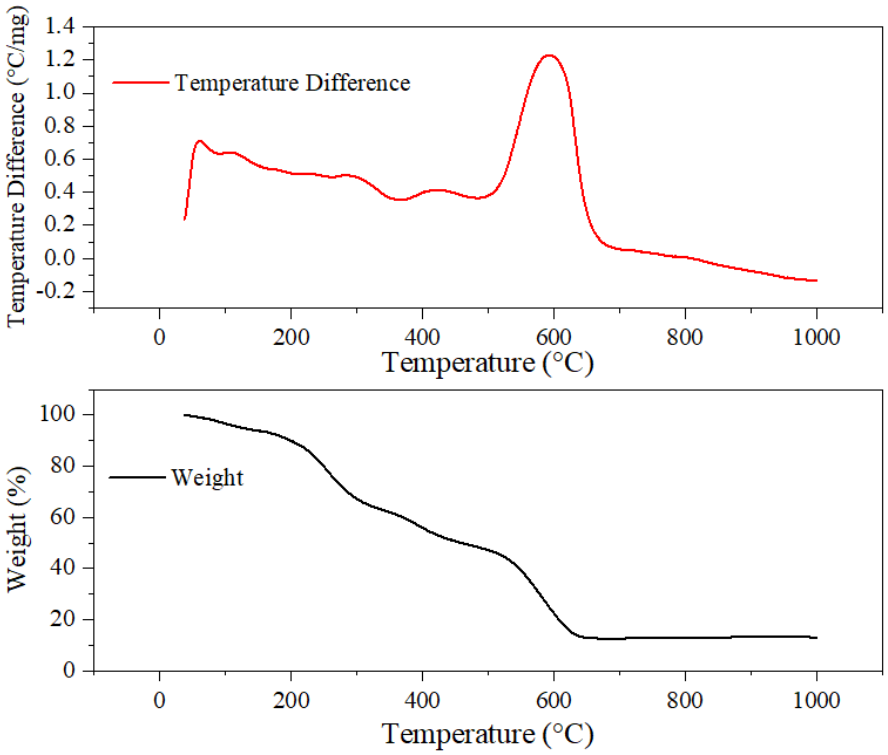

Fig. 1. DTA and TG curves of the dried gel

3. Results and discussion

Fig. 1 displays the DTA-TG curves of the dried specimen. The loss of physically and chemically adsorbed water is responsible for the wide endothermic peak from ambient temperature to 200 °C, which corresponds to a mass loss of 10 percent. The endothermic peak around 310 °C associated with a mass loss of 30 % may be attributed to the decomposition of aluminum and nickel nitrites. The large exothermic peak around 590 °C may be due to the decomposition of polyacrylamide gel [17]. A total weight loss of 87 % was observed in the dried specimen. The TG curve shows no further weight loss at temperatures higher than 620 °C, indicating that the organic species have been completely removed from the sample.

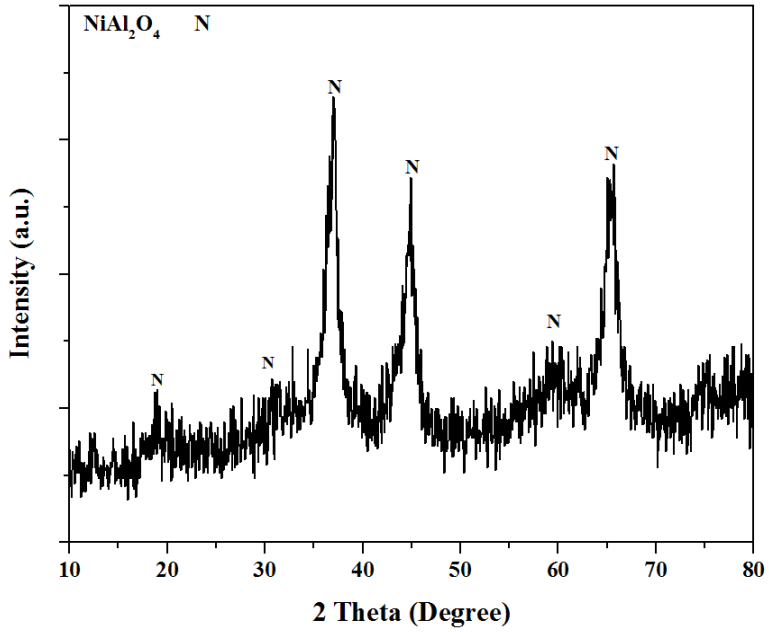

Fig. 2. XRD pattern of the calcined sample at 800 °C

Fig. 2 shows the XRD pattern of the specimen calcined at 800 °C for 2h. The pattern comprises the peaks that were diffracted from crystal planes of the sample and confirms the none-amorphous nature of the powders. XRD pattern agrees with that of spinel nickel aluminate crystallite phase (JCPDS pattern No. 00-010-0339) because the $NiAl_2O_4$ shows typical diffraction peaks which positioned at 2θ values of 37.1, 45, 59.7, and 65.5 degrees. The Scherrer equation (Eq. 2) was used to assess the crystallite size due to the peak broadening based on the XRD data [18].

$$d = \frac{K\lambda}{\beta \cos\theta} \qquad \text{(Eq. 2)}$$

The crystallite size d (nm) has an inverse connection with β (full width at half maximum) and cosθ (the half of the diffraction angle). Furthermore, it demonstrates that the term d has a direct connection with the shape factor (k), which has a common value of 0.9, and the X-ray wavelength (λ). The d was estimated to be 18 nm for the sample.

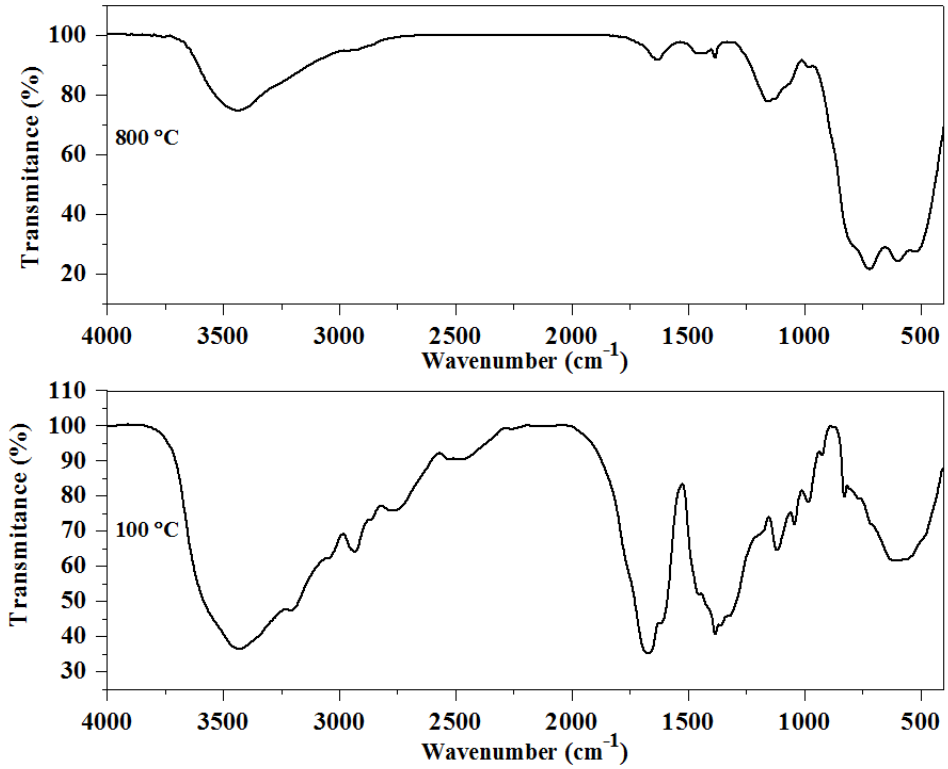

Fig. 3. FTIR spectra of the dried gel and calcined specimen at 800 °C

FTIR results of the dried sample and the sample calcined at 800 °C are shown in Fig. 3. The peaks at 3446 and 1620 cm^{-1} may be attributed to the stretching and bending vibrations of the O–H bond, respectively [19]. The carbon-hydrogen stretching vibration from organic molecules is connected to the absorption band at 2943 cm^{-1}. The COOH stretching vibrations and the peaks pertinent to organic compounds are responsible for the stretching bands between 1000 to 1380 cm^{-1}. However, the band caused by nitrates vibrations could be seen around 1385 cm^{-1} [20]. The peaks related to organic compounds were removed from the samples after calcination. The bands at 724 cm^{-1}, 504 cm^{-1}, and 520 cm^{-1} are connected with the nickel-oxygen, aluminum-oxygen, and nickel-oxygen-aluminum vibration modes, which are seen in both tetrahedral and octahedral situations and indicate the creation of spinel phase structure [21].

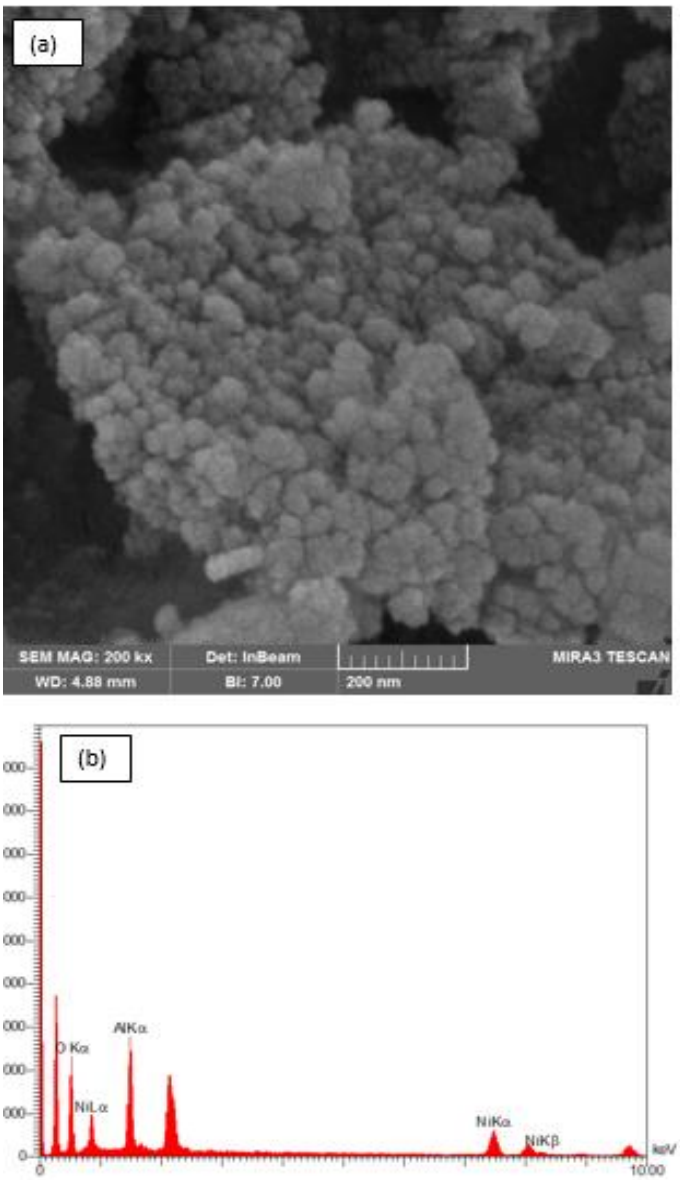

Fig. 4. SEM image (a) and EDS analysis (b) of the calcined sample at 800 °C

SEM was used to examine the morphologies of the $NiAl_2O_4$ nanopowders calcined at 800 °C for 2h, and the result was shown in Fig. 4. As can be seen, the $NiAl_2O_4$ nanoparticles with nanostructure were observed in the SEM image. The powders show a degree of agglomeration. The aggregation of particles is a common phenomenon in nanopowders. This agglomeration can be attributed to the high surface energy of nanoparticles which results in the tendency of the particles to cling to each other for reducing this energy [22]. The EDS analysis taken from the sample shows the existence of Ni, Al, and O elements which confirms the formation of nickel aluminate and proves that there are no impurities in the sample.

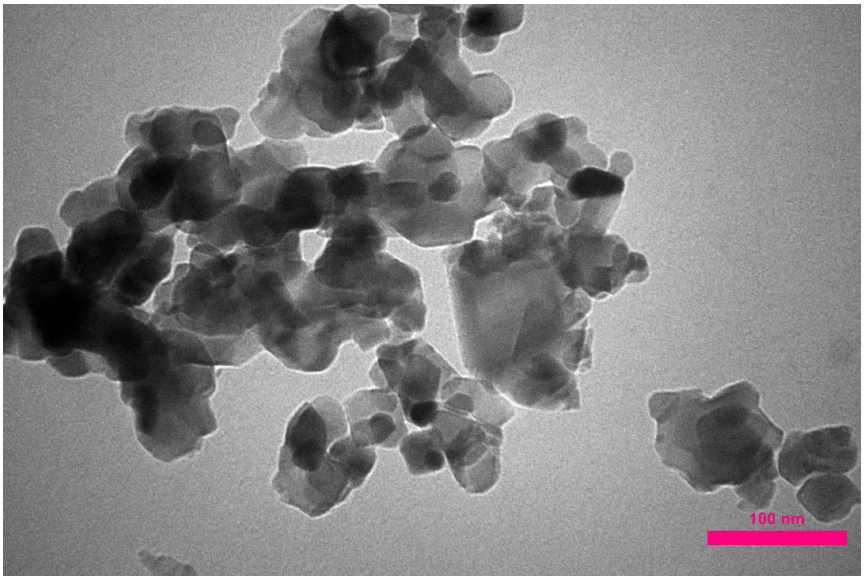

Fig. 5. TEM image of the calcined specimen at 800 °C.

For better observation of the size and morphology of the specimen, transmission electron microscopy (TEM) was utilized, and the result is presented in Fig. 5. As can be seen, the $NiAl_2O_4$ nanoparticles have uniform distribution with both irregular and spherical morphologies with a particle size ranging from 35 to 100 nm. The crystalline size of the samples estimated by the XRD method was smaller than that earned by the TEM image. This difference may be due to the underestimation of the sizes determined by the XRD method because microstrain could affect the results [23,24]. It seems that the formed agglomeration in the present work is lower than those prepared by the combustion method [25]. This lower aggregation may be due to the creation of a polymeric network around the nanoparticles.

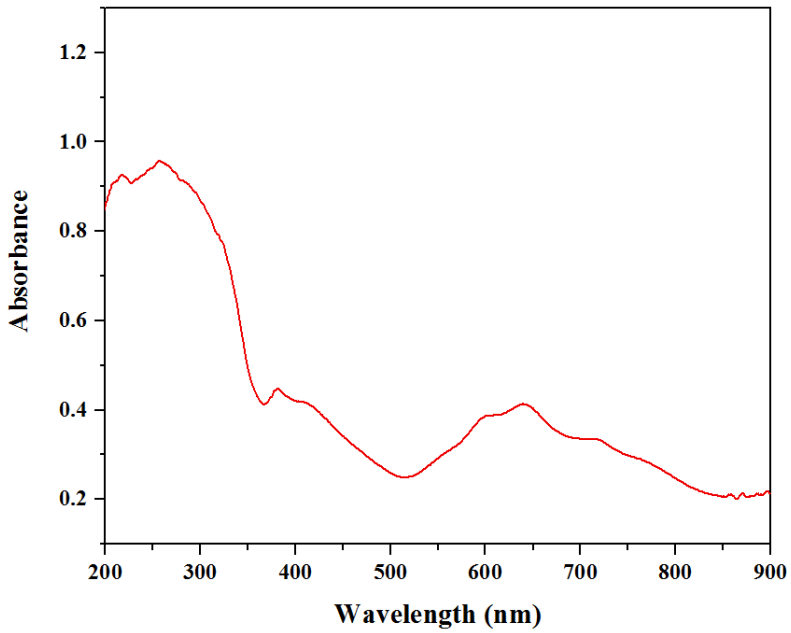

Fig. 6. The absorption spectra obtained in the DRS study of the calcined sample at 800 °C

Diffuse reflectance spectroscopy is commonly used to characterize the optical properties of materials, such as reflectivity, absorption characteristics, and dispersive characteristics. The absorption spectrum of the nickel aluminate is depicted in Fig. 6. Three absorption bands can be seen in the spectra, which are between 230 to 350 nm, 350 to 500 nm, and 500 to 800 nm. The absorption bands 230 to 350 nm, 350 to 500 nm are attributable to charge transfer between metal and oxygen. The $^3T_1(F) \Rightarrow {}^3T_1(P)$, which corresponds to tetrahedrally coordinated nickel ions, is ascribed to the band between 500 to 800 nm [26,27]. The optical bandgap of the material is calculated using the tauc plot (Eq. 3) [28], as shown in Fig. 7.

$$\alpha h\nu = A\left(h\nu - E_g\right)^{\frac{1}{2}} \qquad \text{(Eq. 3)}$$

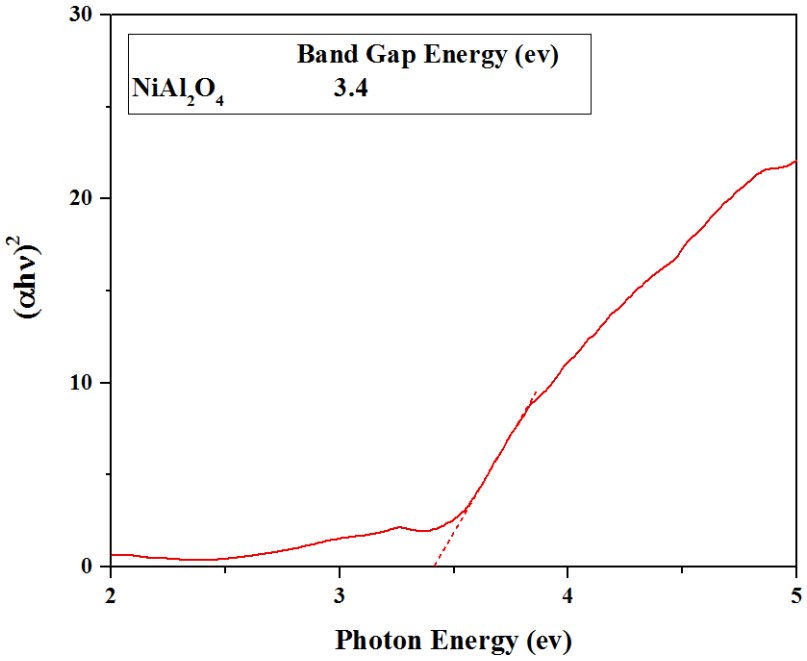

Fig. 7. Tauc plot of $NiAl_2O_4$ nanoparticles calcined at 800 °C

where ν is the light frequency, α is the absorption coefficient, Eg is the optical absorption edge energy, h is the planks constant, and A is a constant. The extrapolation of the curve of $(\alpha h\nu)^2$ versus photon energy (hν) yields the bandgap energy. The bandgap energy of synthesized nickel aluminate was calculated to be 3.44 eV. The bandgap energy is linked to the filled O_{2p} anion valence band and the cationic conduction band formed from the nickel ions [26,29]. The bandgap calculated in the present work was higher than that reported by Elakkiya et al. [26], which was about 3.11 eV. They prepared nickel ferrite nanoparticles via a sol-gel route which shows the method of synthesis has an important effect on the optical properties of $NiAl_2O_4$.

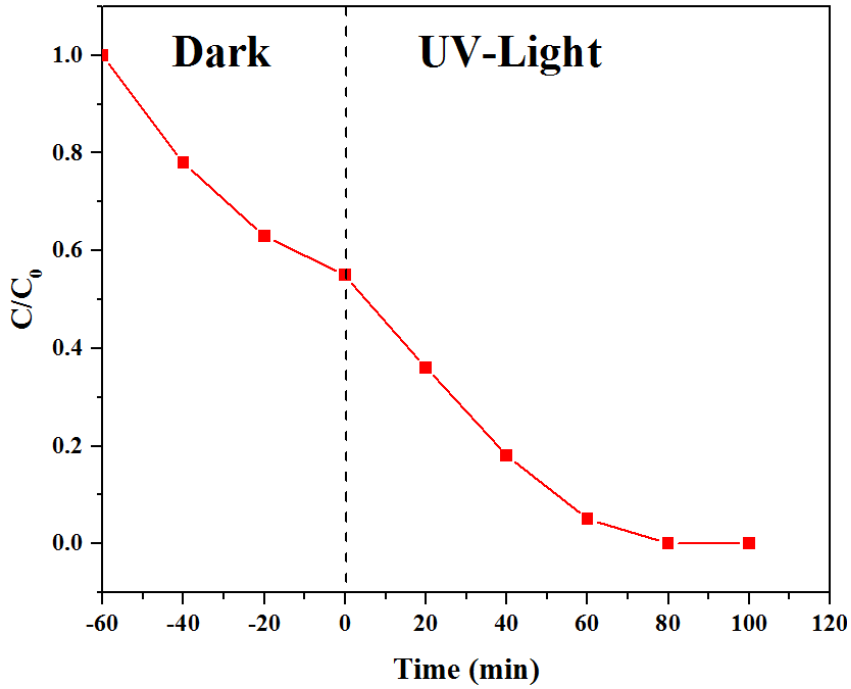

Fig. 8. The degradation curve of the methylene blue in the presence of nickel aluminate nanoparticles.

The degradation of methylene blue under UV irradiation was used to assess the photocatalytic activity of the nickel aluminate samples. Fig. 8 depicts the amount of methylene blue removal as a function of time. The use of $NiAl_2O_4$ nanoparticles results in the significant removal of organic dye. This removal comprises two parts. First, the samples were put in a dark medium to reach to equilibrium adsorption of dyes on the surface of the samples. As can be seen, half of the organic dye was removed via

the adsorption phenomenon. However, after the illumination of the UV light, the removal of methylene blue reach 99%, which is due to the photocatalytic activity of nickel aluminate. In the presence of UV light, the photocatalytic mechanism of the synthesized $NiAl_2O_4$ nanopowders could be described as below. Reactive specious of electron and hole were produced via striking of UV light to the surface of samples. The photogenerated electrons react with oxygen molecules to form peroxide and superoxide species, which subsequently react with water to form hydroxyl radicals. Furthermore, photogenerated holes in the solution may interact with H_2O and form ˙OH. These reactive specious, which have a strong oxidizing capacity, can oxidize methylene blue and produce less dangerous compounds like CO_2 and H_2O [30–32].

Langmuir–Hinshelwood kinetic equation (Eq. 4) [33] can be utilized to explain the photodegradation of methylene blue.

$$-\ln\left(\frac{C}{C_0}\right) = kt \qquad \text{(Eq. 4)}$$

where Co and C are the methylene blue amounts at times t_0 and t. The k is the reaction rate constant. The curve of $\ln(C_0/Ct)$ versus irradiation time of the nickel aluminate sample was plotted as shown in Fig. 9. The first-order K constant was calculated to be 0.035, for the synthesized specimen.

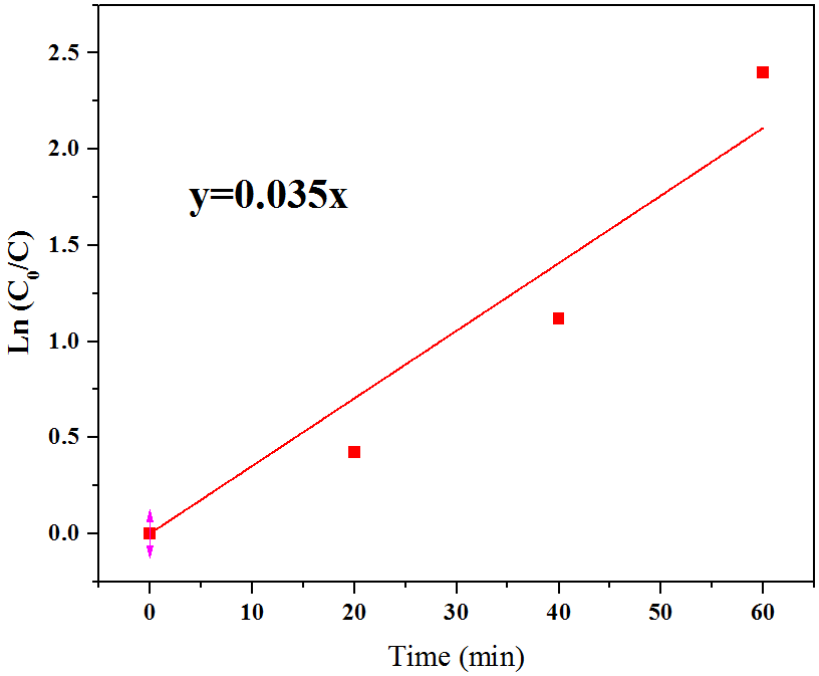

Fig. 9. The $\ln(C_0/C_t)$ versus irradiation time of the nickel aluminate for methylene blue degradation

4. Conclusion

A polymer-assisted gel method was utilized for synthesizing $NiAl_2O_4$ nanopowder that exhibits proper photocatalytic properties for photodegradation of methylene blue as a water pollutant model. XRD results confirmed the synthesize of nickel aluminate with spinel structure for the samples calcined at 800 °C. SEM and TEM findings exhibited that the powders have a nanosized scale with some degree of agglomeration, which is common in nanoparticles. The calculated bandgap of samples was 3.44 eV. The synthesized samples had both adsorption and photocatalytic properties. The produced nickel aluminate calcined at 800 °C could have a methylene blue removal efficiency of about 99%.

References

[1] Z. Mengting, T.A. Kurniawan, S. Fei, T. Ouyang, M.H.D. Othman, M. Rezakazemi, S. Shirazian, Applicability of $BaTiO_3$/graphene oxide (GO) composite for enhanced photodegradation of methylene blue (MB) in synthetic wastewater under UV–vis irradiation, Environ. Pollut. 255 (2019) 113182.

[2] A.A. Shah, M.A. Bhatti, A. Tahira, A.D. Chandio, I.A. Channa, A.G. Sahito, E. Chalangar, M. Willander, O. Nur, Z.H. Ibupoto, Facile synthesis of copper doped ZnO nanorods for the efficient photo degradation of methylene blue and methyl orange, Ceram. Int. 46 (2020) 9997–10005.

[3] M. Saleem, J. Iqbal, A. Nawaz, B. Islam, I. Hussain, Synthesis, characterization, and performance evaluation of pristine and cerium-doped WO_3 nanoparticles for photodegradation of methylene blue via solar irradiation, Int. J. Appl. Ceram. Technol. 17 (2020) 1918–1929.

[4] K.K. Chenab, B. Sohrabi, A. Jafari, S.

Ramakrishna, Water treatment: Functional nanomaterials and applications from adsorption to photodegradation, Mater. Today Chem. 16 (2020) 100262.
[5] S. Yu, Y. Wang, F. Sun, R. Wang, Y. Zhou, Novel mpg-C_3N_4/TiO_2 nanocomposite photocatalytic membrane reactor for sulfamethoxazole photodegradation, Chem. Eng. J. 337 (2018) 183–192.
[6] X. Hu, G. Wang, J. Wang, Z. Hu, Y. Su, Step-scheme NiO/BiOI heterojunction photocatalyst for rhodamine photodegradation, Appl. Surf. Sci. 511 (2020) 145499.
[7] M.H. Aghaali, S. Firoozi, Enhancing the catalytic performance of Co substituted $NiAl_2O_4$ spinel by ultrasonic spray pyrolysis method for steam and dry reforming of methane, Int. J. Hydrogen Energy. 46 (2021) 357–373.
[8] A. Morales-Marín, J.L. Ayastuy, U. Iriarte-Velasco, M.A. Gutiérrez-Ortiz, Biohydrogen production by glycerol Aqueous-Phase Reforming: Effect of promoters (Ce or Mg) in the $NiAl_2O_4$ spinel-derived catalysts, J. Environ. Chem. Eng. 9 (2021) 106433.
[9] M.R.I. Faruque, E. Ahamed, M.A. Rahman, M.T. Islam, Flexible nickel aluminate ($NiAl_2O_4$) based dual-band double negative metamaterial for microwave applications, Results Phys. 14 (2019) 102524.
[10] N.M.D. Vitorino, A. V Kovalevsky, M.C. Ferro, J.C.C. Abrantes, J.R. Frade, Design of $NiAl_2O_4$ cellular monoliths for catalytic applications, Mater. Des. 117 (2017) 332–337.
[11] C. Chen, M. Xu, K. Zhang, H. An, G. Zhang, B. Hong, J. Li, Y. Lai, Atomically ordered and epitaxially grown surface structure in core-shell NCA/$NiAl_2O_4$ enabling high voltage cyclic stability for cathode application, Electrochim. Acta. 300 (2019) 437–444.
[12] S.G. Menon, H.C. Swart, Microwave-assisted synthesis of blue-green $NiAl_2O_4$ nanoparticle pigments with high near-infrared reflectance for indoor cooling, J. Alloys Compd. 819 (2020) 152991.
[13] R. Pournajaf, S.A. Hassanzadeh-Tabrizi, Polyacrylamide synthesis of nanostructured copper aluminate for photocatalytic application, J. Adv. Mater. Process. 5 (2018) 12–19.
[14] S. Wang, D. Li, C. Yang, G. Sun, J. Zhang, Y. Xia, C. Xie, G. Yang, M. Zhou, W. Liu, A novel method for the synthesize of nanostructured $MgFe_2O_4$ photocatalysts, J. Sol-Gel Sci. Technol. 84 (2017) 169–179.
[15] S. Wang, S. Tang, H. Gao, L. Fang, Q. Hu, G. Sun, X. Chen, C. Yu, H. Liu, X. Pan, Modified polyacrylamide gel synthesis of CeO_2 nanoparticles by using cerium sulfate as metal source and its optical and photoluminescence properties, J. Mater. Sci. Mater. Electron. 32 (2021) 10820–10834.
[16] M. Ahmadyari-Sharamin, S.A. Hassanzadeh-Tabrizi, Polyacrylamide gel synthesis, characterization, and optical properties of $Co_{1-x}NixCr_2O_4$ spinel nanopigment, J. Sol-Gel Sci. Technol. 99 (2021) 534–545.
[17] X. Su, G. Bai, J. Zhang, J. Zhou, Y. Jia, Preparation and flash sintering of $MgTiO_3$ nanopowders obtained by the polyacrylamide gel method, Appl. Surf. Sci. 442 (2018) 12–19.
[18] M.A.R. Miranda, J.M. Sasaki, The limit of application of the Scherrer equation, Acta Crystallogr. Sect. A Found. Adv. 74 (2018) 54–65.
[19] M. Łączka, K. Cholewa-Kowalska, K. Kulgawczyk, M. Klisch, W. Mozgawa, Structural examinations of gel-derived materials of the CaO–P_2O_5–SiO_2 system, J. Mol. Struct. 511 (1999) 223–231.
[20] R. Balasubramanian, R. Srinivasan, J. Lee, Barrier, rheological, and antimicrobial properties of sustainable nanocomposites based on gellan gum/polyacrylamide/zinc oxide, Polym. Eng. Sci. 61 (2021) 2477–2486.
[21] F. Majid, J. Rauf, S. Ata, I. Bibi, A. Malik, S.M. Ibrahim, A. Ali, M. Iqbal, Synthesis and characterization of $NiFe_2O_4$ ferrite: Sol–gel and hydrothermal synthesis routes effect on magnetic, structural and dielectric characteristics, Mater. Chem. Phys. 258 (2021) 123888.
[22] J.J.H. McCallister, M.D. Gammage, J.W. Keto, M.F. Becker, D. Kovar, Influence of agglomerate morphology on micro cold spray of Ag nanopowders, J. Aerosol Sci. 151 (2021) 105648.
[23] C. Hu, Z. Zhang, H. Liu, P. Gao, Z.L. Wang, Direct synthesis and structure characterization of ultrafine CeO_2 nanoparticles, Nanotechnology. 17 (2006) 5983.
[24] U.Z.M. Zaidi, A.R. Bushroa, R.R. Ghahnavyeh, R. Mahmoodian, Crystallite size and microstrain: XRD line broadening analysis of AgSiN thin films, Pigment Resin Technol. 48 (2019) 473-480.
[25] C. Ragupathi, J.J. Vijaya, L.J. Kennedy, Preparation, characterization and catalytic properties of nickel aluminate nanoparticles: A comparison between conventional and microwave method, J. Saudi Chem. Soc. 21 (2017) S231–S239.
[26] V. Elakkiya, R. Abhishekram, S. Sumathi, Copper doped nickel aluminate: Synthesis, characterisation, optical and colour properties, Chinese J. Chem. Eng. 27 (2019) 2596–2605.
[27] F.Z. Akika, M. Benamira, H. Lahmar, A. Tibera, R. Chabi, I. Avramova, Ş. Suzer, M. Trari, Structural and optical properties of Cu-substitution of $NiAl_2O_4$ and their photocatalytic activity towards Congo red under solar light irradiation, J. Photochem.

Photobiol. A Chem. 364 (2018) 542–550.
[28] P.R. Jubu, F.K. Yam, V.M. Igba, K.P. Beh, Tauc-plot scale and extrapolation effect on bandgap estimation from UV–vis–NIR data–a case study of β-Ga_2O_3, J. Solid State Chem. 290 (2020) 121576.
[29] C. Venkataramana, S.M. Botsa, P. Shyamala, R. Muralikrishna, Photocatalytic degradation of polyethylene plastics by $NiAl_2O_4$ spinels-synthesis and characterization, Chemosphere. 265 (2021) 129021.
[30] M. Arunkumar, A.S. Nesaraj, One pot chemical synthesis of ultrafine $NiAl_2O_4$ nanoparticles: physico-chemical properties and photocatalytic degradation of organic dyes under visible light irradiation, Inorg. Nano-Metal Chem. 51 (2021) 910–917.
[31] V. Elakkiya, Y. Agarwal, S. Sumathi, Photocatalytic activity of divalent ion (copper, zinc and magnesium) doped $NiAl_2O_4$, Solid State Sci. 82 (2018) 92–98.
[32] M. Arunkumar, A. Samson Nesaraj, Photocatalytic degradation of malachite green dye using $NiAl_2O_4$ and Co doped $NiAl_2O_4$ nanophotocatalysts prepared by simple one pot wet chemical synthetic route, Iran. J. Catal. 10 (2020) 235–245.
[33] A. Iben Ayad, D. Luart, A. Ould Dris, E. Guénin, Kinetic analysis of 4-nitrophenol reduction by "water-soluble" palladium nanoparticles, Nanomaterials. 10 (2020) 1169.